ADVANCED OPTICAL MATERIALS

Supporting Information

for *Adv. Optical Mater.*, DOI: 10.1002/adom.202000481

Nanoscale Structural and Emission Properties within "Russian Doll"-Type InGaN/AlGaN Quantum Wells

Shaobo Cheng, Zewen Wu, Brian Langelier, Xianghua Kong, Toon Coenen, Sangeetha Hari, Yong-Ho Ra, Roksana Tonny Rashid, Alexandre Pofelski, Hui Yuan, Xing Li, Zetian Mi, Hong Guo, and Gianluigi A. Botton**

Supporting Information

Nanoscale structural and emission properties within "Russian Doll"-type InGaN/AlGaN quantum wells

Shaobo Cheng,[1,†] Zewen Wu,[2,3,†] Brian Langelier,[1] Xianghua Kong,[2,*] Toon Coenen,[4] Sangeetha Hari,[4] Yong-Ho Ra,[5,6] Roksana Tonny Rashid,[5] Alexandre Pofelski,[1] Hui Yuan,[1] Xing Li,[7] Zetian Mi,[5,8] Hong Guo,[2] Gianluigi A. Botton[1,9,*]

1. Canadian Centre for Electron Microscopy and Department of Materials Science and Engineering, McMaster University, Main Street West, Hamilton, Ontario, L8S 4M1, Canada
2. Department of Physics, McGill University, 3480 University Street, Montreal, Quebec H3A 0E9, Canada
3. Beijing Key Laboratory of Nanophotonics and Ultrafine Optoelectronic Systems, School of Physics, Beijing Institute of Technology, 5 Zhongguancun South Street, Beijing 100081, China
4. Delmic, Kanaalweg 4, 2628 EB Delft, The Netherlands
5. Department of Electrical and Computer Engineering, McGill University, 3480 University Street, Montreal, Quebec H3A 0E9, Canada
6. Optic & Electronic Component Material Center, Korea Institute of Ceramic Engineering & Technology, Jinju 52851, Republic of Korea
7. School of Physics and Engineering, Zhengzhou University, Daxue Road 75, Zhengzhou, 450052 China
8. Department of Electrical Engineering and Computer Science, University of Michigan, 1301 Beal Avenue, Ann Arbor, MI 48109, USA
9. Canadian Light Source, 44 Innovation Boulevard Saskatoon, Saskatchewan, S7N 2V3, Canada

1. Strain-induced band gap changes for III-Nitrides

The $k \cdot p$ perturbation approach is employed to calculated strain-induced band gap changes for III-Nitrides based on their DFT calculated band structures. Taking the topmost three valence bands into consideration [53], the transition energy changes E_1, E_2, E_3 induced by strain could be estimated by

$$E_1 = (a_{cz} - D_1)\varepsilon_{zz} + (a_{ct} - D_2)(\varepsilon_{xx} + \varepsilon_{yy}) + D_5(\varepsilon_{xx} - \varepsilon_{yy}) \quad (1)$$

$$E_2 = (a_{cz} - D_1)\varepsilon_{zz} + (a_{ct} - D_2)(\varepsilon_{xx} + \varepsilon_{yy}) - \frac{1}{2}[D_3\varepsilon_{zz} + D_4(\varepsilon_{xx} + \varepsilon_{yy}) + D_5(\varepsilon_{xx} - \varepsilon_{yy})] + \frac{\delta}{2} \quad (2)$$

$$E_3 = (a_{cz} - D_1)\varepsilon_{zz} + (a_{ct} - D_2)(\varepsilon_{xx} + \varepsilon_{yy}) - \frac{1}{2}[D_3\varepsilon_{zz} + D_4(\varepsilon_{xx} + \varepsilon_{yy}) + D_5(\varepsilon_{xx} - \varepsilon_{yy})] - \frac{\delta}{2} \quad (3)$$

where

$$\delta = \sqrt{[D_3\varepsilon_{zz} + D_4(\varepsilon_{xx} + \varepsilon_{yy}) + D_5(\varepsilon_{xx} - \varepsilon_{yy})]^2 + 8D_6^2\varepsilon_{yz}^2} \quad (4)$$

Here a_{cz} and a_{ct} are the deformation potential for the conduction band while D_i denotes the deformation potential for the valence band. All the used deformation potential values of III-Nitrides are taken from the Heyd-Scuseria-Ernzerhof (HSE) hybrid functional results in Ref. 33.

With respect to ternary compound, for example, $In_xGa_{1-x}N$, its deformation potential could be easily obtained by the linear interpolation

$$D_i = x \cdot D_i^{InN} + (1 - x) \cdot D_i^{GaN}$$

ε represents the strain tensor, thereinto, ε_{xx}, ε_{yy} and ε_{zz} are strain components along the *x*, *y* and *z* directions respectively. In our calculations, the *x*, *y* and *z* directions in equations (1-4) were defined as $[11\bar{2}0]$, $[\bar{1}100]$ and [0001] directions of wurtzite III-Nitrides. To distinguish the other coordinates used in the following

method description, we name this coordinate as the natural coordinate with the others as the primed coordinate. From the experimental results shown in Fig. 1c, we found that InGaN is grown on AlGaN, which means that InGaN experience the biaxial stress induced by AlGaN. Since their contact surface changes from $(0\bar{1}12)$ plane into $(0\bar{1}11)$ plane which is different from the xy plane we defined in equations (1-4), strain transform between natural coordinate and primed coordinate is required to get the right ε_{xx}, ε_{yy} and ε_{zz}. The E_i could be calculated from equations (1-3). By combining the transitions energies obtained in free-standing III-Nitrides [49,50], we could calculate and plot their new band gaps under strain as shown in Fig. 4a and Fig. S9.

Strain components calculation

As stated above and shown in Fig. 1c, InGaN was grown on AlGaN, thus InGaN experienced the biaxial stress induced by the lattice mismatch between InGaN and AlGaN. For any contacting interface (plane OBC as shown in Fig. S11), the lattice mismatch ε_{m1}, ε_{m2} could be calculated by the equations below:

$$\varepsilon_{m1} = \frac{CD_T - CD_L}{CD_L}$$

$$\varepsilon_{m2} = \frac{OB_T - OB_L}{OB_L}$$

$$CD_L = a_{InGaN}$$

$$CD_T = a_{AlGaN}$$

$$OB_L = \sqrt{OA_L^2 + AB_L^2}$$

$$OA_L = \sqrt{3}a_{InGaN}$$

$$AB_L = \frac{c_L}{c_{AlGaN}}\sqrt{3}a_{InGaN}\tan\theta$$

$$OB_T = \frac{\sqrt{3}a_{InGaN}}{\cos\theta}$$

Here *a* and *c* are the lattice parameters of wurtzite III-Nitrides. For ternary alloy, for example, $In_xGa_{1-x}N$, according to Vegard's law, we can get the values of *a* and *c* by following the equation below:

$$a_{InGaN} = x \cdot a_{InN} + (1-x) \cdot a_{GaN}$$

$$c_{InGaN} = x \cdot c_{InN} + (1-x) \cdot c_{GaN}$$

θ is the angle between the contacting interface (between InGaN and AlGaN) and the *xy* plane defined in the natural coordinate. The geometric schematic is plotted in Fig. S11 for a better illustration.

In order to obtain the strain components in the natural coordinate, the primed coordinate (*x'*, *y'* and *z'* directions) needs to be defined. First, they share the same origin of coordinates and the same *x* direction, and the *x'y'* plane is defined as the contacting interface between InGaN and AlGaN. Naturally, the *z'* direction could be confirmed according to the right-hand screw rule. Thus, in this primed coordinate, for InGaN, we have

$$\varepsilon_{x'x'} = \varepsilon_{m1} \quad (5)$$

$$\varepsilon_{y'y'} = \varepsilon_{m2} \quad (6)$$

$$\varepsilon_{x'y'} = 0 \quad (7)$$

Since there is no stress and shear strain along *z'* direction, we find

$$\sigma_{z'z'} = 0 \quad (8)$$

$$\sigma_{x'z'} = 0 \quad (9)$$

$$\sigma_{y'z'} = 0 \quad (10)$$

According to Ref. 51, the stress transform between natural coordinate and primed coordinate can be displayed as follows,

$$\sigma_{x'x'} = \sigma_{xx} \tag{11}$$

$$\sigma_{y'y'} = \sigma_{yy}\cos^2\theta + \sigma_{zz}\sin^2\theta - \sigma_{yz}\sin 2\theta \tag{12}$$

$$\sigma_{z'z'} = \sigma_{yy}\sin^2\theta + \sigma_{zz}\cos^2\theta + \sigma_{yz}\sin 2\theta \tag{13}$$

$$\sigma_{y'z'} = \frac{1}{2}(\sigma_{yy} - \sigma_{zz})\sin 2\theta + \sigma_{yz}\cos 2\theta \tag{14}$$

$$\sigma_{x'z'} = \sigma_{xy}\cos\theta + \sigma_{xy}\sin\theta \tag{15}$$

$$\sigma_{x'y'} = \sigma_{xy}\cos\theta - \sigma_{xz}\sin\theta \tag{16}$$

We can transform the strain components from the primed coordinate to the natural coordinate by using the following equations:

$$\varepsilon_{xx} = \varepsilon_{x'x'} \tag{17}$$

$$\varepsilon_{yy} = \varepsilon_{y'y'}\cos^2\theta + \varepsilon_{z'z'}\sin^2\theta + \varepsilon_{y'z'}\sin 2\theta \tag{18}$$

$$\varepsilon_{zz} = \varepsilon_{y'y'}\sin^2\theta + \varepsilon_{z'z'}\cos^2\theta + \varepsilon_{y'z'}\sin 2\theta \tag{19}$$

$$\varepsilon_{yz} = \frac{1}{2}\left(\varepsilon_{z'z'} - \varepsilon_{y'y'}\right)\sin\theta + \varepsilon_{y'z'}\cos 2\theta \tag{20}$$

$$\varepsilon_{xz} = \varepsilon_{x'z'}\cos\theta - \varepsilon_{x'y'}\sin\theta \tag{21}$$

$$\varepsilon_{xy} = \varepsilon_{x'y'}\cos\theta + \varepsilon_{x'z'}\sin\theta \tag{22}$$

Additionally, in natural coordinate, Hooke's law can be used to link the stress and strain.

$$\sigma_{xx} = C_{11}\varepsilon_{xx} + C_{12}\varepsilon_{yy} + C_{13}\varepsilon_{zz} \tag{23}$$

$$\sigma_{yy} = C_{12}\varepsilon_{xx} + C_{11}\varepsilon_{yy} + C_{13}\varepsilon_{zz} \tag{24}$$

$$\sigma_{zz} = C_{13}\varepsilon_{xx} + C_{13}\varepsilon_{yy} + C_{33}\varepsilon_{zz} \tag{25}$$

$$\sigma_{yz} = 2C_{44}\varepsilon_{yz} \tag{26}$$

$$\sigma_{xz} = 2C_{44}\varepsilon_{xz} \tag{27}$$

$$\sigma_{xy} = \left(C_{11} - C_{12}\right)\varepsilon_{xy} \tag{28}$$

Bringing equations (17-28) into equations (11-16), we can obtain the stress-strain tensor equations in the primed coordinate. By combining with equations (5-10), we can calculate all the strain components in the primed coordinate:

$$\varepsilon_{x'x'} = \varepsilon_{m1} \tag{29}$$

$$\varepsilon_{y'y'} = \varepsilon_{m2} \tag{30}$$

$$\varepsilon_{z'z'} = \frac{\left(B_{41}\varepsilon_{m1} + B_{42}\varepsilon_{m2}\right)A_{32} - \left(B_{31}\varepsilon_{m1} + B_{32}\varepsilon_{m2}\right)A_{42}}{A_{31}A_{42} - A_{32}A_{41}} \tag{31}$$

$$\varepsilon_{y'z'} = \frac{\left(B_{31}\varepsilon_{m1} + B_{32}\varepsilon_{m2}\right)A_{41} - \left(B_{41}\varepsilon_{m1} + B_{42}\varepsilon_{m2}\right)A_{31}}{A_{31}A_{42} - A_{32}A_{41}} \tag{32}$$

where

$$A_{31} = C_{11}\sin^4\theta + \left(\frac{1}{2}C_{13} + C_{44}\right)\sin^2 2\theta + C_{33}\cos^4\theta$$

$$A_{32} = \left[C_{11}\sin^2\theta + \left(C_{13} + 2C_{44}\right)\cos 2\theta - C_{33}\cos^2\theta\right]\sin 2\theta$$

$$A_{41} = \frac{1}{2}\left[\left(C_{11} - C_{13}\right)\sin^2\theta + 2C_{44}\cos 2\theta + \left(C_{13} - C_{33}\right)\cos^2\theta\right]\sin 2\theta$$

$$A_{42} = \left(\frac{C_{11} + C_{33}}{2} - C_{13}\right)\sin^2 2\theta + 2C_{44}\cos^2 2\theta$$

$$B_{31} = C_{11}\sin^2\theta + C_{13}\cos^2\theta$$

$$B_{32} = C_{13}\left(\sin^4\theta + \cos^4\theta\right) + \left(\frac{C_{11} + C_{33}}{4} - C_{44}\right)\sin^2 2\theta$$

$$B_{41} = \left(\frac{C_{12} - C_{13}}{4}\right)\sin 2\theta$$

$$B_{42} = \frac{1}{2}\left[C_{11}\cos^2\theta - \left(C_{13} + 2C_{44}\right)\cos 2\theta - C_{33}\sin^2\theta\right]\sin 2\theta$$

C_{ij} corresponds to the elastic constant of III-Nitrides. The value of C_{ij} in our calculations is taken from Ref. 52. For $In_xGa_{1-x}N$, the elastic constants could be easily obtained by the linear interpolation, similar to the deformation potential.

$$C_{ij} = x \cdot C_{ij}^{InN} + (1-x) \cdot C_{ij}^{GaN}$$

Combining equations (29-32) with equations (17-22), ε_{xx}, ε_{yy}, ε_{zz}, and ε_{yz} in the natural coordinate can thus be obtained.

Therefore, we are able to calculate the interfacial lattice mismatch induced band gap changes in III-Nitrides.

2. Nanorods components analysis

Combing the experimental results shown in Fig. 2c, Fig. 3b, Fig. S6a and Fig. S6b, we obtained the specific compound-compositions of the nanorod based on the DFT results of the light emission spectrum evolution along with different Indium doping levels plotted in Fig. 4a, Fig. S7a and Fig. S9. During these data analyses, the ratio of element N is always set as 50%, and we didn't take the results of the atomic ratio for N element plotted in Fig. 3b since theoretically the ratio of element N should always be 50% no matter in $In_xGa_{1-x}N$ or in $Al_xGa_{1-x}N$. The fluctuations of the atomic ratio for N element shown in Fig. 3b could be contributed by measuring error or disorders in the nanorod.

3. Figures and Tables

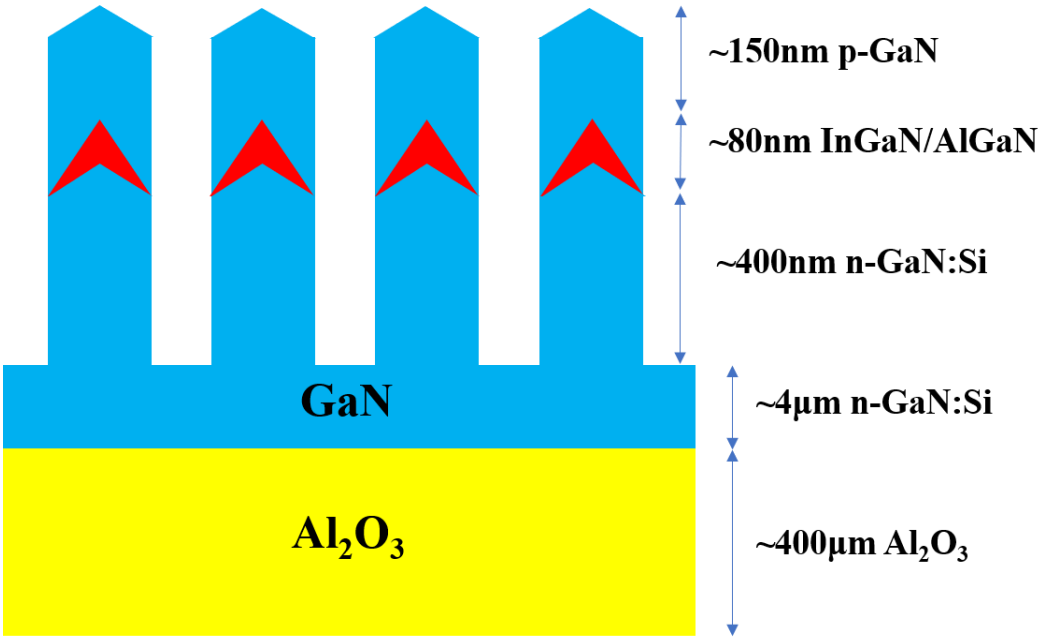

Figure S1. Schematic diagram of GaN nanorod fabricated on Al_2O_3 substrate. The

eight layers of InGaN/AlGaN are shown in red.

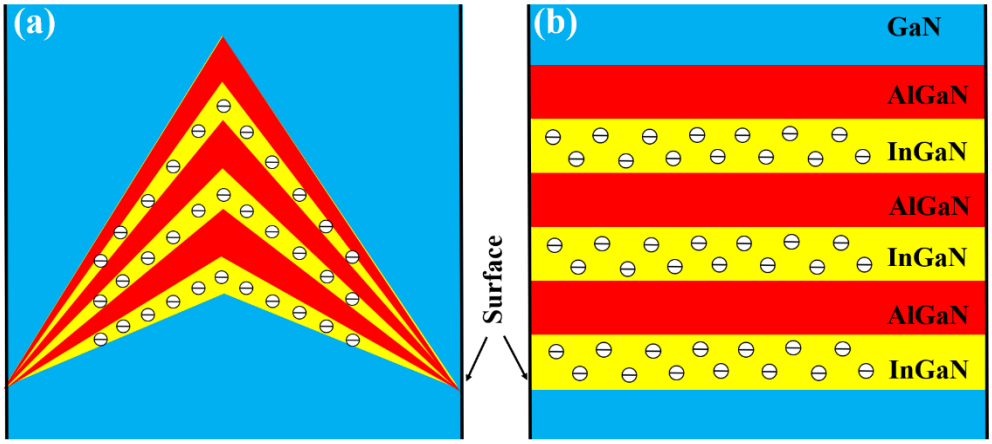

Figure S2. Schematic diagrams showing (a) the boomerang shape and (b) planar configuration of InGaN/AlGaN. The green, red, and yellow color represent GaN, AlGaN, and InGaN, respectively. The InGaN and AlGaN layers converge at the bottom corners and restrict the carriers in InGaN layers from recombining with the surface defects.

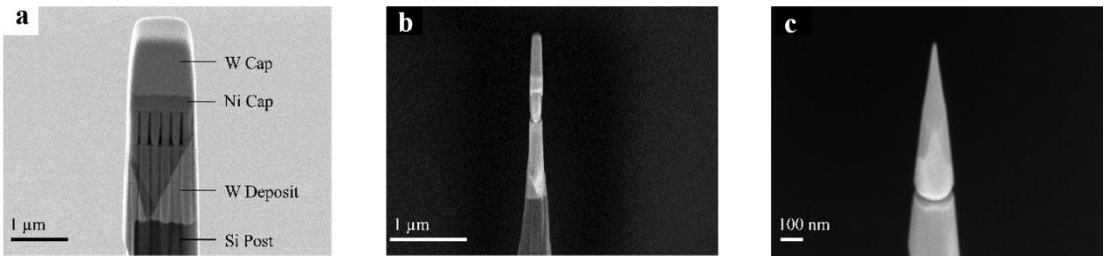

Figure S3. Preparation of APT samples using FIB. (a) Nanorod samples still attached to the substrate material are mounted onto pre-sharpened Si microposts using W deposition, while Ni and W caps protect the nanorods from the high-current FIB beam. (b) The sample is sharpened so only a single nanorod remains on the micropost. (c) Low-kV FIB milling is used to mill past the W and Ni capping layers, and produce a sharp tip.

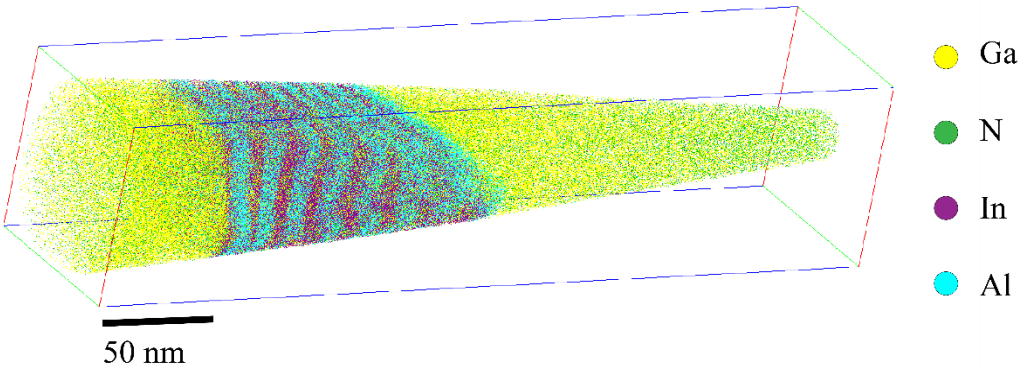

Figure S4. 3D atom map of APT data showing Ga, N, In, and Al ions (3 %, 15 %, 27 %, and 69 % of detected ions displayed, respectively, for the purpose of visualization).

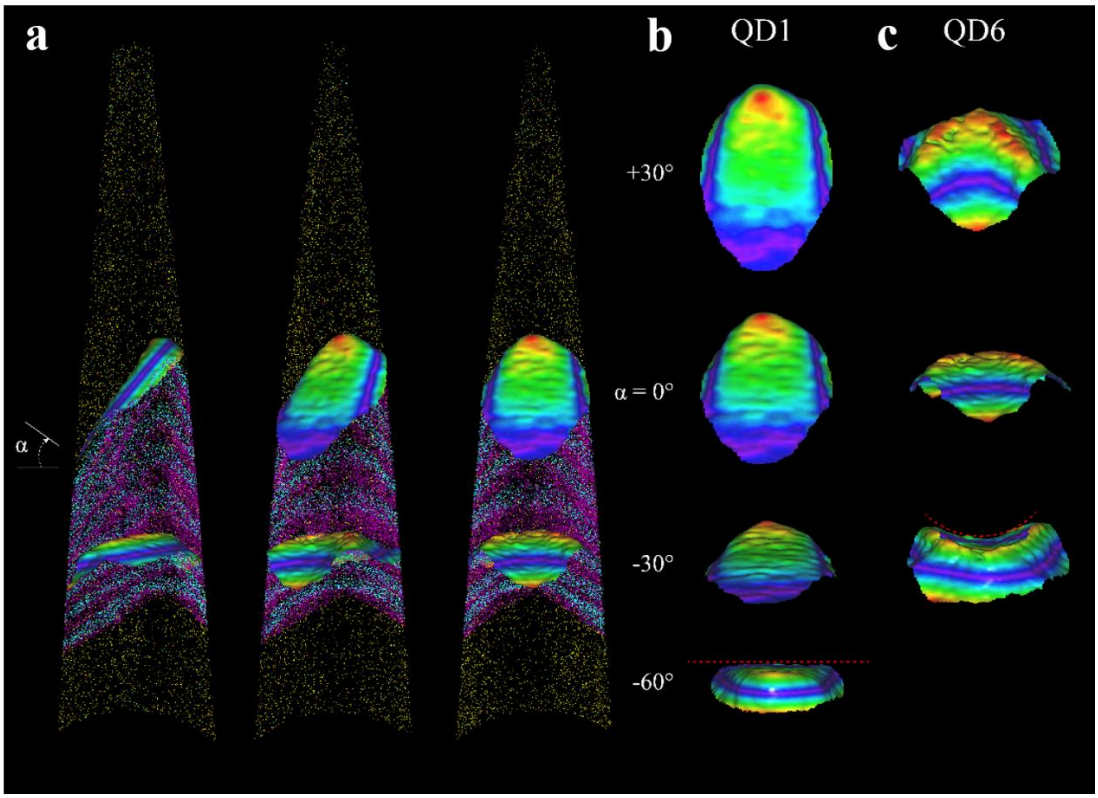

Figure S5. The shape of the AlGaN layers extracted from APT results. (a) Surfaces defined by Al concentration in the AlGaN layers for QP 1 and 6 are shown with the APT data. The color maps on the surfaces are defined by the distance from a medial "best-fit" plane at each surface. (b)(c) Images of QP1 and QP 6 surfaces, respectively, with different viewing angles (α) as defined in a, showing the different features of the planes. QP 1 shows planar faceting, while the surface for QP 6 reveals curved surfaces

along each facet.

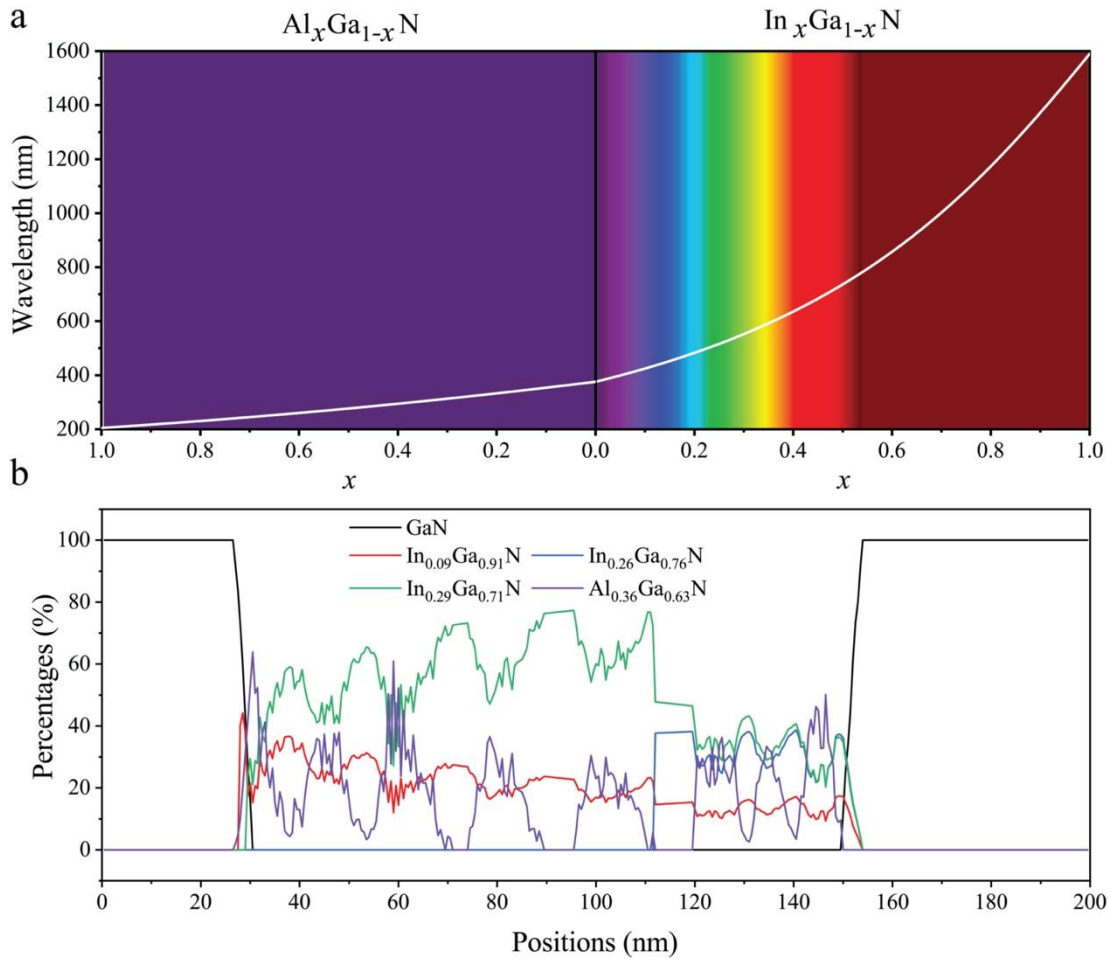

Figure S6. Light emission and nanorods components analysis. (a) Wavelength of light emission spectra in $Al_xGa_{1-x}N$ and $In_xGa_{1-x}N$ without considering the strain effects. Infrared light is marked as dark red (the right most part), and ultraviolet light is marked as dark purple (the left most part). The white curve depicts the light emission spectrum evolution along with different doping levels. (b) The percentage distribution of different compounds in the nanorod. The X-axis is the same as the Y-axis in Figure 3b.

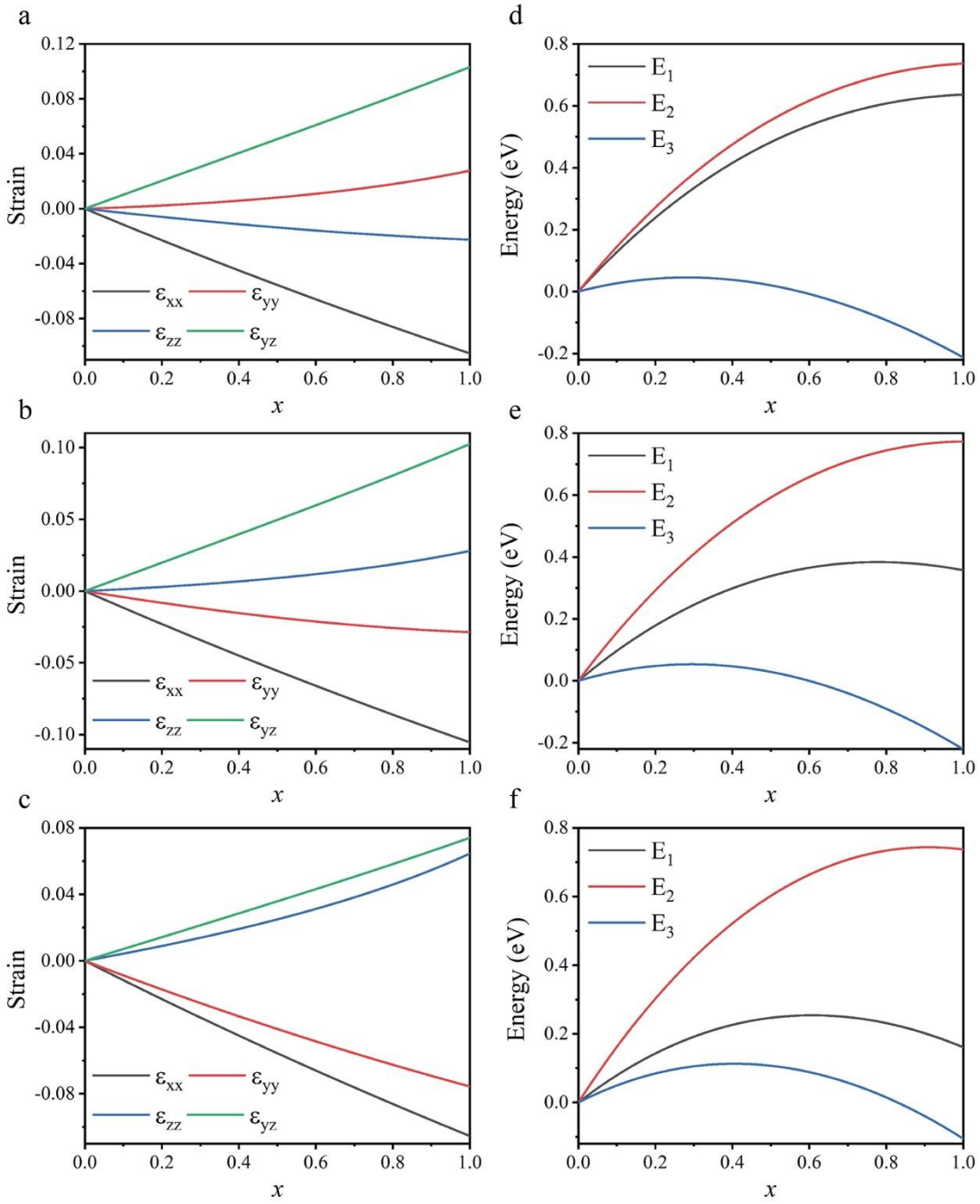

Figure S7. Effects of strain on the bandgap of InGaN. (a)(b)(c) Strain components experienced by $In_xGa_{1-x}N$ induced by lattice mismatch between InGaN ($0\bar{2}21$) and AlGaN ($0\bar{2}21$), InGaN ($0\bar{1}11$) and AlGaN ($0\bar{1}11$), InGaN ($0\bar{1}12$) and AlGaN ($0\bar{1}12$). (d)(e)(f) Corresponding transition energy changes to the strain components in (a)(b)(c).

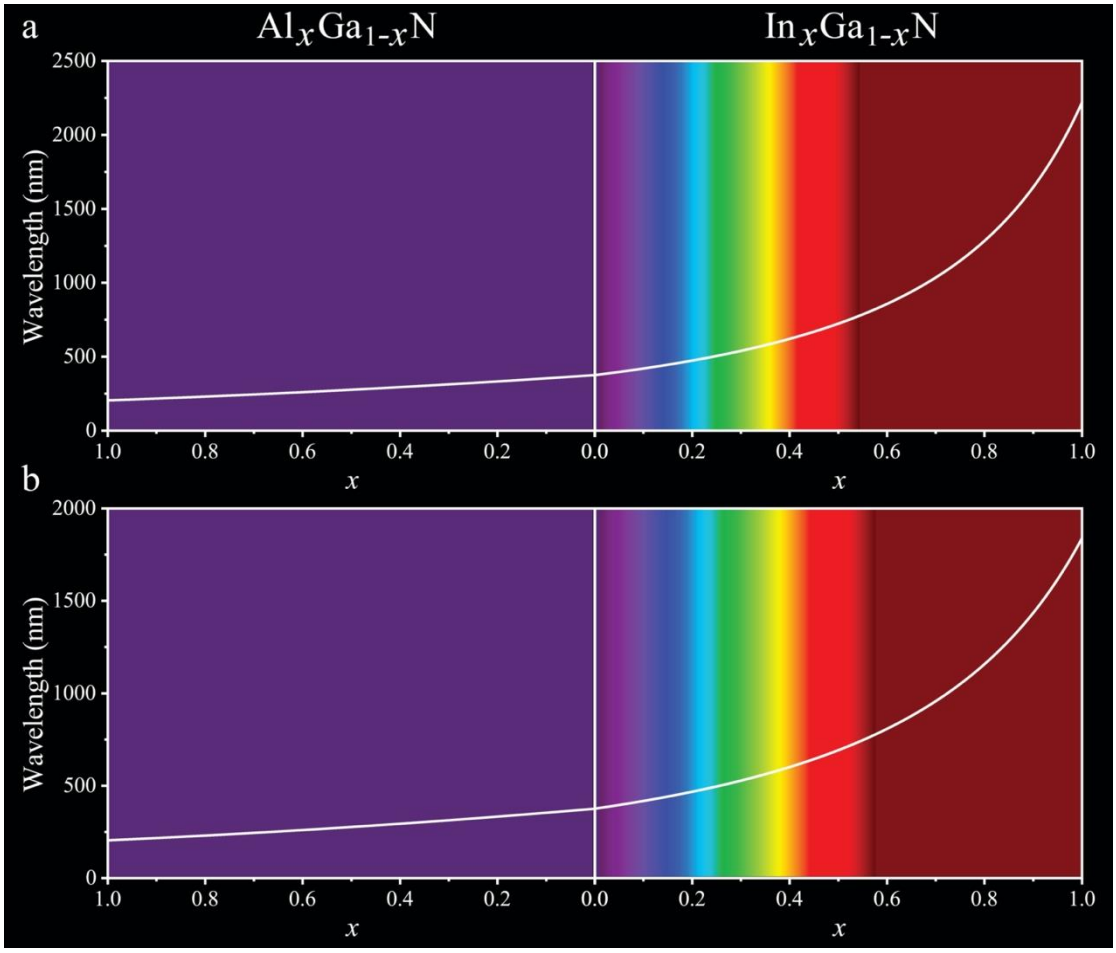

Figure S8. Light emission spectra in $Al_xGa_{1-x}N$ and $In_xGa_{1-x}N$. (a) Emission wavelength in $In_xGa_{1-x}N$ where biaxial stress induced by the lattice mismatch between InGaN ($0\bar{1}11$) and AlGaN ($0\bar{1}11$) are taken into consideration. (b) Emission wavelength in $In_xGa_{1-x}N$ where biaxial stress induced by the lattice mismatch between InGaN ($0\bar{1}12$) and AlGaN ($0\bar{1}12$) are taken into consideration.

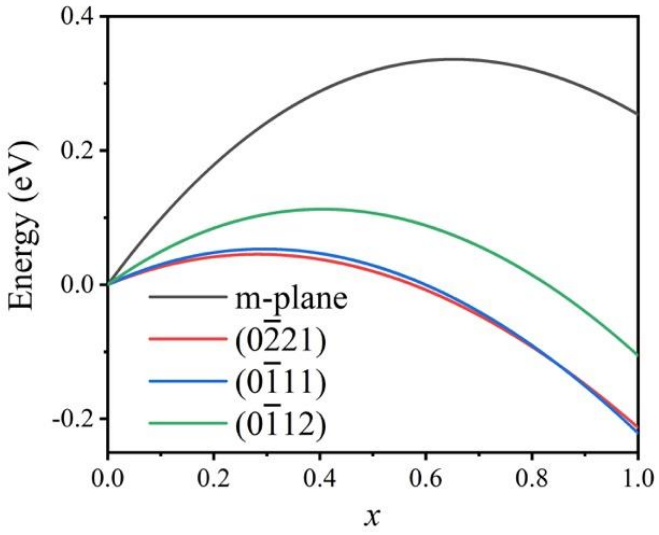

Figure S9. Energy changes E_3 for $In_xGa_{1-x}N$ grown on four different AlGaN planes. Black line corresponding to M-plane describes nonpolar plane while the others are semipolar ones. If E_3 is positive, it means there is an increase for the bandgap of $In_xGa_{1-x}N$, and a decrease for the bandgap of $In_xGa_{1-x}N$ for the negative values.

Table S1. Strain components (ε_{ij}, i, j=x, y, z) and bandgap changes (E_k, k=1, 2, 3) for different $In_xGa_{1-x}N$ compounds grown on different substrate planes.

plane	component	ε_{xx}	ε_{yy}	ε_{zz}	ε_{yz}	E_1	E_2	E_3
(0$\bar{2}$21)	$In_{0.10}Ga_{0.90}N$	-0.011	0.00095	-0.0028	0.0095	0.012	0.014	0.025
	$In_{0.26}Ga_{0.74}N$	-0.030	0.0032	-0.0075	0.026	0.29	0.36	0.045
	$In_{0.29}Ga_{0.71}N$	-0.035	0.0038	-0.0085	0.030	0.33	0.38	0.045
(0$\bar{1}$11)	$In_{0.09}Ga_{0.91}N$	-0.011	-0.0040	0.0013	0.0093	0.092	0.15	0.029
	$In_{0.26}Ga_{0.74}N$	-0.030	-0.010	0.0039	0.026	0.22	0.36	0.052
	$In_{0.30}Ga_{0.70}N$	-0.034	-0.012	0.0046	0.029	0.24	0.41	0.053
(0 $\bar{1}$12)	$In_{0.10}Ga_{0.90}N$	-0.012	-0.0088	0.0044	0.0072	0.079	0.16	0.049
	$In_{0.27}Ga_{0.73}N$	-0.031	-0.023	0.013	0.020	0.18	0.39	0.10
	$In_{0.31}Ga_{0.69}N$	-0.036	-0.027	0.015	0.022	0.20	0.44	0.10

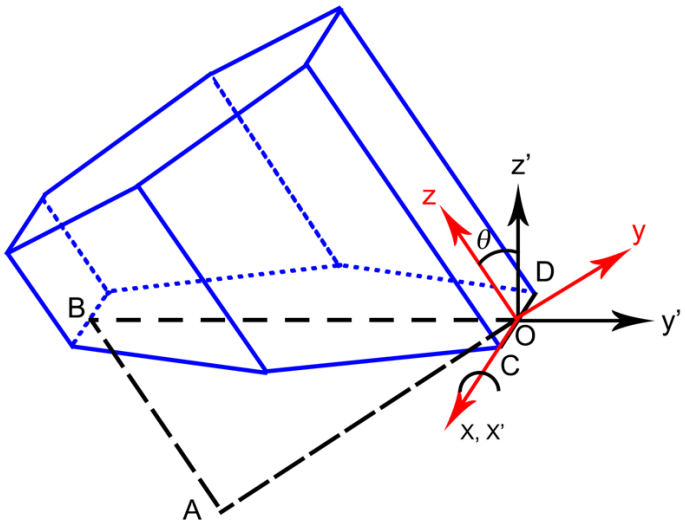

Figure S10. Schematic for the determination of crystal lattice mismatch between InGaN and AlGaN (or GaN). The x'y' plane (OBC plane) is defined as the contacting interface between InGaN and AlGaN. Naturally, the z' direction could be confirmed according to the right-hand screw rule.